



**HAL**  
open science

## Deep Argo reveals Bottom Water properties and pathways in the Australian-Antarctic basin

Annie Foppert, Stephen R. Rintoul, Sarah G. Purkey, Nathalie Zilberman, Taiyo Kobayashi, Jean-Baptiste Sallée, Esmee M. Wijk, Luke O. Wallace

### ► To cite this version:

Annie Foppert, Stephen R. Rintoul, Sarah G. Purkey, Nathalie Zilberman, Taiyo Kobayashi, et al.. Deep Argo reveals Bottom Water properties and pathways in the Australian-Antarctic basin. *Journal of Geophysical Research. Oceans*, 2021, 126 (12), pp.e2021JC017935. 10.1029/2021JC017935 . hal-03560251

**HAL Id: hal-03560251**

**<https://hal.science/hal-03560251>**








Submitted on 20 Aug 2022

**HAL** is a multi-disciplinary open access archive for the deposit and dissemination of scientific research documents, whether they are published or not. The documents may come from teaching and research institutions in France or abroad, or from public or private research centers.

L'archive ouverte pluridisciplinaire **HAL**, est destinée au dépôt et à la diffusion de documents scientifiques de niveau recherche, publiés ou non, émanant des établissements d'enseignement et de recherche français ou étrangers, des laboratoires publics ou privés.

Copyright

## Deep Argo Reveals Bottom Water Properties and Pathways in the Australian-Antarctic Basin

Annie Foppert<sup>1,2</sup> , Stephen R. Rintoul<sup>1,2,3,4</sup> , Sarah G. Purkey<sup>5</sup> , Nathalie Zilberman<sup>5</sup> , Taiyo Kobayashi<sup>6</sup> , Jean-Baptiste Sallée<sup>7</sup> , Esmee M. van Wijk<sup>1,3</sup> , and Luke O. Wallace<sup>8</sup>

<sup>1</sup>Australian Antarctic Program Partnership, Hobart, TAS, Australia, <sup>2</sup>Institute for Marine and Antarctic Studies, University of Tasmania, Hobart, TAS, Australia, <sup>3</sup>CSIRO Oceans and Atmosphere, Hobart, TAS, Australia, <sup>4</sup>Centre for Southern Hemisphere Oceans Research, Hobart, TAS, Australia, <sup>5</sup>Scripps Institution of Oceanography, UCSD, San Diego, CA, USA, <sup>6</sup>Japan Agency for Marine-Earth Science and Technology, Yokosuka, Japan, <sup>7</sup>Sorbonne Université, CNRS/IRD/MNHN, LOCEAN, IPSL, Paris, France, <sup>8</sup>School of Geography, Planning and Spatial Sciences, University of Tasmania, Hobart, TAS, Australia

### Key Points:

- Deep Argo floats map Antarctic Bottom Water properties year-round and under-ice in the Australian-Antarctic Basin from 2018 to 2020
- Floats reveal Antarctic Bottom Water (AABW) pathways in unprecedented detail and show some Ross Sea Bottom Water hugs the slope and some descends to the deep ocean
- Pulses of Adélie Land Bottom Water descending the slope interact with Ross Sea and Bottom Water (RSBW) and drive short-term (~1 day) variability near 140°E

### Correspondence to:

A. Foppert,  
[annie.foppert@utas.edu.au](mailto:annie.foppert@utas.edu.au)

### Citation:

Foppert, A., Rintoul, S. R., Purkey, S. G., Zilberman, N., Kobayashi, T., Sallée, J.-B., et al. (2021). Deep Argo reveals bottom water properties and pathways in the Australian-Antarctic Basin. *Journal of Geophysical Research: Oceans*, 126, e2021JC017935. <https://doi.org/10.1029/2021JC017935>

Received 23 AUG 2021

Accepted 11 DEC 2021

**Abstract** Changes in properties and quantity of Antarctic Bottom Water (AABW) have major implications for the climate system, through sequestration of heat and carbon into, and ventilation of, the abyssal ocean. Yet, it remains one of the most difficult water masses to observe. An array of 12 Deep Argo floats, capable of profiling from the surface to the seafloor and under sea ice, provides a new perspective on AABW in the Australian-Antarctic Basin. Over 2 years of data from the floats illuminate AABW properties with unprecedented detail, simultaneously sampling AABW at multiple locations, year-round, throughout the basin. Calibrating each float individually with nearby, quasi-simultaneous shipboard profiles ensures the highest quality salinity data, with estimated accuracy of  $\pm 0.005$  or better. Pathways of Ross Sea and Adélie Land Bottom Water (RSBW and ALBW), defined by their unique temperature and salinity characteristics, are mapped along the continental slope from their respective sources. The main pathway of RSBW, identified by its characteristic deep salinity maximum, is inferred to be inshore of the 3,700 m isobath, where it cools and freshens westward along the slope before interacting with ALBW near 140°E. A pulse of very cold and very fresh (nearly  $-0.6^{\circ}\text{C}$ ,  $34.82\text{ g kg}^{-1}$ ) ALBW appears in February 2019, highlighting temporal variability on daily scales near its source. Deep Argo has greatly enhanced our view of AABW in the Australian-Antarctic Basin and will prove to be an essential tool for monitoring future changes in the deep ocean by drastically increasing observations in a cost-effective way.

**Plain Language Summary** Antarctic Bottom Water (AABW) is both a crucially important component of Earth's climate, with the capacity to store heat and carbon in the abyssal ocean for centuries, and one of the hardest water masses to monitor. New instruments have been developed to do just that. Deep Argo floats are able to take measurements of temperature and salinity from the surface to seafloor and can continue to profile safely while under winter sea ice. 12 Deep Argo floats were deployed in the Australian-Antarctic Basin and have been continuously profiling for over two years, producing an unprecedented observational data set of AABW properties. We map out pathways of AABW from two source regions: the Ross Sea and Adélie Land. The Ross Sea Bottom Water tends to flow westward hugging the slope, but there is some leakage into the deeper ocean. Near 140°E, Adélie Land Bottom Water flows down the slope, sometimes in pulses, usually slicing under Ross Sea Bottom Water and through a narrow bathymetric saddle between a seamount and the slope. Deep Argo floats offer a window into the deep ocean, enhancing our understanding of AABW and allowing for continuous monitoring of its variability.

## 1. Introduction

The production and export of Antarctic Bottom Water (AABW) acts as the southernmost and deepest limb of the global meridional overturning circulation, regulating climate through ventilation of the abyssal ocean and sequestration of anthropogenic heat and carbon from the atmosphere. Long-term trends based on repeat hydrography transects across the Southern Ocean show a freshening, warming, and contraction of these deepest and densest waters over the past several decades (Purkey & Johnson, 2010, 2012, 2013). These trends are especially strong in the Australian-Antarctic Basin (AAB, Aoki et al., 2005, 2013; Menezes et al., 2017; Shimada et al., 2012; van Wijk & Rintoul, 2014). AABW has warmed by near  $0.05^{\circ}\text{C}$  per decade in waters deeper than 4,000 m (Purkey &

Johnson, 2010) and freshened by about  $-0.01$  psu per decade in the deepest 300 m of the water column (van Wijk & Rintoul, 2014). The observed variability in AABW properties could reflect a change in the properties of Dense Shelf Water (DSW), changes in the formation and export of DSW, changes in the mixing ratio between DSW and Circumpolar Deep Water (CDW), or some combination of all three processes.

DSW produced in the Ross Sea and along the Adélie Land coast mixes with CDW to supply AABW to the AAB, accounting for 40% of the total AABW produced globally (Gordon & Tchernia, 1978; Orsi et al., 1999; Rintoul, 1998). Observed multidecadal changes in AABW properties in the AAB have been attributed to changes in these sources of DSW. The freshening trend is strongest near the source regions, with about  $-0.03$  per decade in Ross Sea DSW (Jacobs & Giulivi, 2010), and becomes progressively weaker along its outflow path (van Wijk & Rintoul, 2014). However, recent work has shown a rapid rebound in Ross Sea DSW salinity over the past several years, that is, between 2014 and 2018, to values last seen in the mid-late 1990s (Castagno et al., 2019) and the subsequent AABW exported from the Ross Sea (Silvano et al., 2020). In fact, a reversal of the long-term freshening trend has been documented throughout the AAB (Aoki et al., 2020; Thomas et al., 2020).

Limited observations, in both space and time, make it difficult to fully resolve and understand changes in the AABW properties in the AAB. The multidecadal trends found by several studies (e.g., Purkey & Johnson, 2010, 2012, 2013; van Wijk & Rintoul, 2014) are based on spatially and temporally sparse hydrographic surveys, sometimes taken a decade apart, and thus too coarse to resolve inter- and intra-annual variability. Moreover, Kobayashi (2018) showed a contraction of the AABW layer 4–5 times faster than the trends from the 1990s, based on 20 months of data from deep-profiling floats deployed near Adélie Land from 2012 to 2014. Note that this was soon after the calving of the Mertz Glacier Tongue, which significantly changed the icescape on the continental shelf, thereby altering AABW formation and its carbon uptake (Shadwick et al., 2013). Relatively rapid changes in AABW properties driven by local changes in forcing over the continental shelf, for example, changes in Adélie Land Bottom Water (ALBW) driven by the Mertz Glacier Tongue calving (Snow et al., 2018) and changes in Ross Sea Bottom Water (RSBW) driven by regional climate anomalies (Silvano et al., 2020), highlight the superimposition of shorter-term variability on the long-term trends and the need for continuous monitoring of AABW.

A pilot array of Deep Argo floats in the AAB helps put the apparent multi-decadal temporal trends and variability in context by providing observations of AABW properties and pathways with high resolution in space and time. The floats have transmitted more than two years of CTD profiles, most reaching the seafloor and including profiles taken under sea ice. These data provide year-round information from the eastern AAB and capture spatial and temporal variability of AABW not seen before. This data set also allows for an unprecedented representation of the pathways and interactions of RSBW and ALBW.

The Deep Argo float data and complementary shipboard hydrography are described in the following section. Section 3 details our estimation method for under-ice profiles that lack GPS position data and the post-deployment calibration of salinity profiles. Section 4 describes the analyses used. The results are presented in Section 5 by outlining the spatial and temporal variability of AABW properties in the AAB, and presenting a case study on high frequency, small-scale variability near  $140^{\circ}\text{E}$ . A discussion of the work, including a synopsis of the pathways of RSBW and ALBW, is found in Section 6, and is followed by a brief conclusion in Section 7.

## 2. Data

### 2.1. Deep Argo Pilot Array in the AAB

The pilot array in the AAB consists of 12 active Deep Argo floats equipped with SeaBird Scientific (SBE) CTD sensors (Figure 1). There are eight Deep SOLO floats, each with a SBE-61 CTD capable of profiling to 6,000 dbar, five floats manufactured by Scripps Institution of Oceanography and three by MRV Systems (Roemmich et al., 2019). There are three Deep Arvor floats designed by Ifremer and manufactured by NKE Instrumentation (Le Reste et al., 2016) and one Deep NINJA float developed by JAMSTEC and TSK (Kobayashi et al., 2013), each with an extended-depth SBE-41CP CTD capable of profiling to 4,000 dbar. All 12 floats have a bottom-detection system, allowing them to safely profile to the seafloor. The three MRV Deep SOLO floats were deployed in Austral summer 2019 from R/V *Kaiyo-Maru*, while all other floats were deployed in Austral summer 2018 from R/V *Investigator*. More details about the floats and their deployments can be found in Table 1.

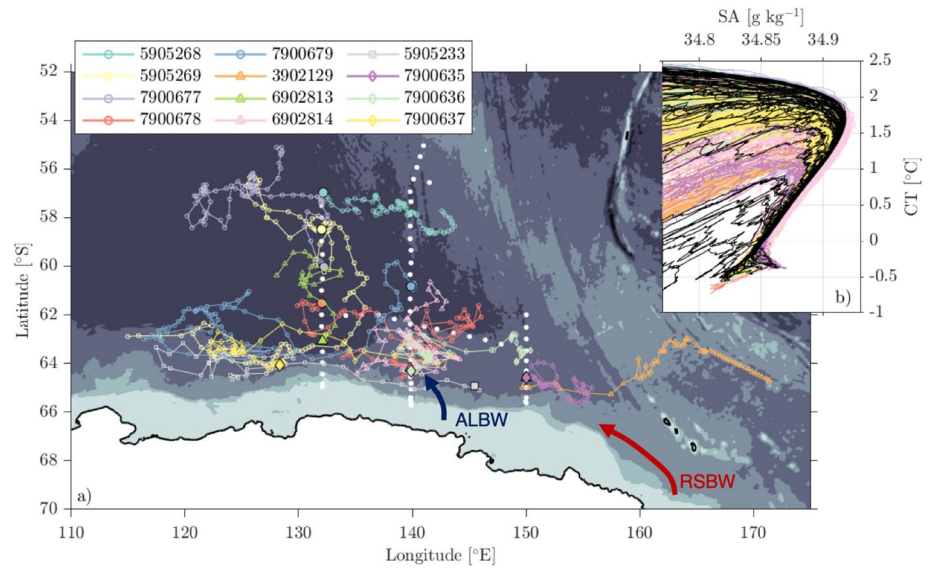


**Figure 1.** Deep Argo pilot array in the Australian-Antarctic Basin (AAB). (a) All Deep Argo profiles are shown by colored symbols, with each symbol representing an individual float and the larger filled symbols outlined in black represent deployment locations. The SIO Deep SOLO floats are represented by circles, Deep Arvor floats by triangles, Deep NINJA float by squares, and MRV Deep SOLO floats by diamonds. Float WMO identification numbers are provided in the legend. Shipboard CTD locations from 2018 used for calibrating the floats are represented by the small white dots. Bathymetry from ETOPO2v2 is contoured every 1,000 m and the Antarctic coast is shown by the thick black line. The outflows of Ross Sea Bottom Water (RSBW) and Adélie Land Bottom Water (ALBW) are shown schematically with red and blue arrows, respectively. (b) CTD profiles from the AAB, shown in panel a, as a function of conservative temperature and absolute salinity (i.e., in  $CT$ - $SA$  space). Colored lines represent post-calibration Deep Argo data after calibration and under-ice navigation, with colors matching the symbols in panel (a). Black lines represent the 2018 shipboard hydrography (white dots in panel a). Note that the two floats that exhibited a small drift in salinity (7900679 and 5905233) are included in the map but not in the  $CT$ - $SA$  diagram.

The practical salinity ( $SP$ ) of each float is calibrated against a nearby ship-based profile (details of the calibration in Section 3.2). Any anomalously fresh spikes in bottom salinity, that is, a decrease in salinity greater than 0.01 relative to adjacent waters, is removed from the profiles. These anomalously fresh spikes at the bottom of some profiles are likely due to fouling of the conductivity sensor by deep-sea sediment and do not appear to affect the subsequent profiles. Standard hydrographic variables, for example, conservative temperature ( $CT$  [ $^{\circ}C$ ]), absolute

**Table 1**  
Deep Argo Float Details and Deployment Information

Float type	CTD ( $P_{max}$ capability)	Deployment R/V	WMO ID	Latitude ( $^{\circ}S$ )	Longitude ( $^{\circ}E$ )	Date
Scripps Deep SOLO	SBE-61 (6,000 dbar)	<i>Investigator</i>	5905268	56.97	132.17	16 February 2018
			5905269	58.50	131.99	15 February 2018
			7900677	60.03	132.23	15 February 2018
			7900678	61.51	132.01	14 February 2018
			7900679	60.84	139.87	27 January 2018
Deep Arvor	SBE-41CP (4,000 dbar)	<i>Investigator</i>	3902129	64.60	150.00	04 February 2018
			6902813	63.09	132.11	11 February 2018
			6902814	64.22	139.83	30 January 2018
Deep NINJA	SBE-41CP (4,000 dbar)	<i>Investigator</i>	5905233	64.94	145.44	03 February 2018
MRV Deep SOLO	SBE-61 (6,000 dbar)	<i>Kaiyo-Maru</i>	7900635	64.59	150.00	27 January 2019
			7900636	64.29	139.87	03 February 2019
			7900637	64.05	128.37	12 February 2019

salinity ( $SA$  [ $\text{g kg}^{-1}$ ]), and neutral density ( $\gamma^N$  [ $\text{kg m}^{-3}$ ]) – are computed directly from the calibrated and de-spiked CTD data (Jackett & McDougall, 1997; McDougall & Barker, 2011).

One Deep Argo float (Deep Arvor #6902813) exhibits an obvious drift in salinity after 8 months of profiling, and we exclude profiles after the drift begins. That is, practical salinity on the in-situ  $0.5^\circ\text{C}$  isotherm increased nearly linearly by about 0.035 psu from October 2018 to June 2020, while all other floats have a scatter within  $\pm 0.005$  psu on the  $0.5^\circ\text{C}$  isotherm (not shown). All profiles taken by this float after 15 October 2018 are not considered here. Note that two other floats showed less substantial, but significant, fresh drifts of close to 0.01 psu during the beginning of their deployments (Deep SOLO #7900679 and NINJA #5905233; not shown). The drift in salinity is assumed constant with pressure, that is, the entire profile would exhibit a constant offset. Thus, the shape of the profile in  $CT$ - $SA$  space still provides useful information about the presence or absence of RSBW. Data from these two floats are therefore neglected throughout the study, except when taking a detailed look at the pathways of AABW (and the locations of these profiles are included in Figure 1).

We consider 855 high-quality profiles from the Deep Argo array collected from January 2018 through June 2020, of which nearly 600 reached the seafloor (including the two floats that exhibited small but significant drifts). If no grounding flag exists, we assume the float has profiled to the seafloor if its maximum pressure is less than the configured profile pressure by at least 100 dbar; for profiles with known position data, we assume it has profiled to the seafloor if both the maximum pressure and the pressure at the seafloor calculated from bathymetry is less than the configured profile pressure. After several initial shallow profiles taken at high frequency to verify that the floats are working, the sampling cycle is increased to about 10 days. Yet, each float's drift time is configurable, such that the cycle times vary during a float's lifetime and were as long as 20 days in the AAB pilot array (with one exception where 30 days passed between two profiles made by Deep Arvor #6902814). Additionally, one float profiled at near daily frequency for the first month of its deployment. The floats' parking pressures, another configurable variable, were set between 2000 dbar and 4,500 dbar after the initial testing period, such that the floats generally remained in the AAB. However, Deep Arvor #3902129, configured to park at 2,500 dbar, was carried east out of the basin by the deep-reaching flow of the Antarctic Circumpolar Current (orange triangles, Figure 1).

This pilot array has dramatically increased the number of profiles taken in the AAB. For comparison, there are 756 profiles to deeper than 2,000 m over a similar region ( $55^\circ$ – $65.5^\circ\text{S}$ ,  $110^\circ$ – $175^\circ\text{E}$ ; 1960–2017) in the World Ocean Database 2018 (Boyer et al., 2018), and less than 10% of those were taken in winter (May through October). The array is even more impressive if we focus on the southern part of the basin ( $60^\circ$ – $65.5^\circ\text{S}$ ,  $110^\circ$ – $160^\circ\text{E}$ ), where the database has only 351 profiles to greater than 3,000 m and 31 of which are from winter. The Deep Argo array alone has measured 572 profiles from the same area, 397 of which have reached the seafloor. The array has provided 217 winter profiles from this region and 163 of those winter profiles are to the seafloor. That is, in only two and a half years, the array has exceeded the total number of historical profiles in the southern AAB, and provided more than a five-fold increase in the number of winter profiles.

## 2.2. Shipboard Observations

Float observations of AABW properties in the AAB are compared to historical shipboard observations. In particular, we compare AABW properties along, or in the vicinity of  $150^\circ\text{E}$  and  $140^\circ\text{E}$  where repeat shipboard transects began the early 1990s during the World Ocean Circulation Experiment and have continued through the GO-SHIP era. Repeat transect SR3 along  $140^\circ\text{E}$  is one of the most frequently occupied GO-SHIP section, with nine occupations used in this study, including data from the 2018 deployment voyage on the *R/V Investigator*. There are some additional regional measurements dating back to 1969–1971 taken by USNS *Eltanin* (Gordon & Tchernia, 1978). Measurements taken from the 1990s and on were collected to meet the standards of the WOCE Hydrographic Program (Joyce, 1994), with accuracies for temperature within  $\pm 0.002^\circ\text{C}$  and for salinity within  $\pm 0.002$  psu. Measurements taken prior from the *Eltanin* are less certain, and are thought to have accuracies closer to  $\pm 0.004^\circ\text{C}$  for temperature and between  $\pm 0.003$  psu and 0.01 psu for salinity, however the exact accuracies for those data are not known (van Wijk & Rintoul, 2014).

### 2.3. Bathymetry

Seafloor bathymetry is provided by the ETOPO2v2 database (National Geophysical Data Center, 2006). This 2-min gridded global bathymetry product gives seafloor depth throughout the AAB and allows for adjustment of position data from bottom-reaching under-ice profiles (see Section 3.1 for details).

## 3. Postdeployment Float Data Processing

### 3.1. Navigation of Under-Ice Profiles

Under-ice profiles do not have GPS position data and therefore the location of these profiles is not known. The position of under-ice profiles is typically linearly interpolated, however this technique is less accurate over longer gaps (i.e., several months). Therefore, the positions of under-ice Deep SOLO profiles are determined through the bathymetry-constrained navigation method of Wallace et al. (2020). This method, originally developed for floats parked on the continental shelf, finds the shortest feasible path during the under-ice period by requiring grounded profiles with an unknown position, to meet a bathymetry constraint. It first limits the location of the float to be within areas where the difference between the maximum depth of the float and known bathymetry is less than 40 m. The location is further refined under the assumption that the float took the shortest path between the depth restrained areas. This path is determined by iteratively reducing the distance a float can move between cycles. The iterative process is repeated forwards and backwards along the path until the area in which a cycle is predicted to have occurred reaches below a threshold area. The location of the cycle is then taken the center point of the predicted area.

The positions of under-ice Deep Arvor and Deep NINJA profiles are first linearly interpolated between the last known positions. The positions of bottom-reaching profiles are further refined by adjusting the latitude, such that the maximum pressure matches the pressure at the seafloor calculated from the bathymetry data. We cannot use the iterative method of Wallace et al. (2020) for these floats, because they do not reach the seafloor in regions deeper than 4,000 m. Thus, a simple latitudinal adjustment, of no more than  $0.5^\circ$ , is done to the bottom-reaching profiles to match the seafloor pressure as closely as possible. Profiles that do not extend to the seafloor are linearly interpolated between the last known or adjusted positions.

Yamazaki et al. (2020) used a similar terrain-following method, albeit more complex, and estimated errors by applying their method to profiles with known positions over self-imposed position data gaps of varying cycles/times. Those authors found a position error of  $23 \pm 27$  km for a 90-day gap, and that the latitudinal and longitudinal errors exceeded 50 km after about 25–30 cycles. These errors are the same as errors found by using a linear interpolation, yet the terrain-following method excludes the possibility of having a contradiction between maximum pressure and seafloor depth. Wallace et al. (2020) performed an error analysis for the method using float data from the continental shelf. The configuration of those floats (parked on the seabed) was such that they had low drift speeds, so the magnitude of the estimated accuracies are not comparable. Yet, their algorithm produced a significant improvement in position accuracy (median accuracy of 2.6 km after a 100-gap compared to 5.9 km when using a linear interpolation). Thus, we suspect a significant improvement in position estimates when applying the algorithm of Wallace et al. (2020) to the Deep Argo pilot array.

### 3.2. Salinity Calibration

A unique pressure dependency correction is calculated for each float's conductivity cell in order to gain the most accurate salinity measurements. This pressure-dependent conductivity, and thus salinity, adjustment factor,  $\epsilon$ , is referred to as the "CP-cor" value. The CP-cor value recommended by SBE for the Deep Argo CTDs,  $\epsilon_{\text{recommended}}$ , is actively being validated and the community is working on deriving the best method for implementing this practice of the global Deep Argo fleet prior to data distribution (Zilberman et al., 2019). However, biases toward fresher values with pressure relative to shipboard reference profiles have been observed (Kobayashi et al., 2021). Therefore, we calculate the pressure dependency based on contemporaneous shipboard CTD profiles and apply them to each float, with the exception of the Deep SOLO floats deployed in 2019 that were calibrated against nearby CTD profiles from the previous year. The newly calibrated practical salinity,  $SP$ , for each float is then calculated from the adjusted conductivity with its pressure-dependent correction applied.

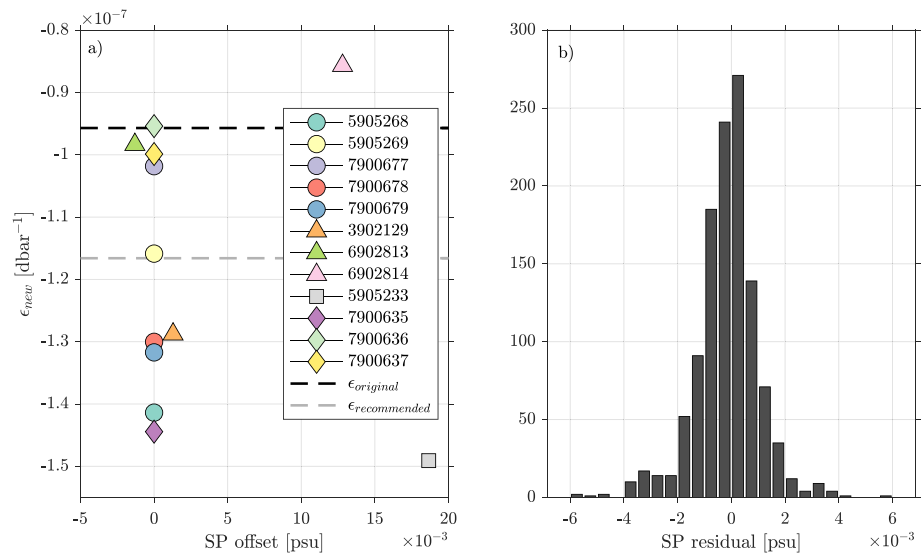


**Figure 2.** Calibration of Deep Argo data. (a) Values of the new pressure-dependent conductivity correction factor,  $\epsilon_{\text{new}}$  ( $\text{dbar}^{-1}$ ), and the constant offset applied float salinity profiles precalibration. Positive offset values represent a fresh bias in float salinity. The shapes and colors are the same as Figure 1a. The black and gray dashed lines represent the original and recommended values of  $\epsilon$  provided by SeaBird Electronics, respectively. (b) Histogram of postcalibration practical salinity residuals for all calibration profiles. The residuals represent the first deep float CTD profile subtracted from the shipboard reference CTD profile on CT isotherms between 1,500 and 2,000 dbar and the deep salinity minimum (i.e., ship-float salinity in the stable part of the water column for the first deep profile).

We use the first deep ( $p_{\text{max}} > 2,000$  dbar) profile from each float to calculate its new CP-cor value,  $\epsilon_{\text{new}}$ , and calibrate its salinity thereafter. The same correction factor is used for every profile taken by each float, such that each float has its own individual  $\epsilon_{\text{new}}$ . We calibrate the profiles based on the stable part of the water column, that is, from either 1,500 or 2,000 dbar to the deep salinity minimum, ensuring the calibration is done over at least 1,000 dbar of the water column. That is, we calibrate the profiles from within the CDW layer to the bottom of the profile, or to above the RSBW layer, where the T-S curves are effectively linear. The details of the calibration, following the procedure of Gregory C. Johnson (Deep Argo workshop, 2019), are as follows:

1. Calculate “conservative conductivity” ( $CCo$ ), that is, conductivity based on conservative temperature ( $CT$ ) and surface pressure, for the first deep float profile and shipboard reference profile.
2. Invert the SBE calibration equation, that is, remove the nominal temperature- and pressure-dependent correction values, to calculate the uncorrected conservative conductivity ( $CCo_{\text{raw}} = CCo \cdot (1 + \delta T + \epsilon p)$ , where  $T$  and  $p$  are the in-situ temperature and pressure measured by the CTD, and  $\delta$  and  $\epsilon$  are the “CTcor” and “CPcor” values, respectively.)
3. Interpolate the shipboard reference  $CCo_{\text{raw}}$  to float  $CT$  values, such that the calibration is done in conservative temperature space, rather than pressure space, to remove effects of isopycnal heaving. Compute the new pressure correction factor ( $\epsilon_{\text{new}}$ ) by minimizing the differences between float and reference  $CCo_{\text{raw}}$  with a linear fit to obtain the optimal  $CCo$  ( $CCo_{\text{opt}}$ ).
4. Solve for  $\epsilon_{\text{new}}$  by rearranging the SBE calibration equation:  $\epsilon_{\text{new}} = ((CCo_{\text{raw}}/CCo_{\text{opt}}) - 1 - \delta T)/p$ . The value of  $\epsilon_{\text{new}}$  for each float is the depth-average  $\epsilon_{\text{new}}$ .
5. Apply  $\epsilon_{\text{new}}$  to all profiles by multiplying the full-depth conductivity by  $(1 + \delta T + \epsilon p)/(1 + \delta T + \epsilon_{\text{new}} p)$  and computing the adjusted  $SP$  for each float individually.

Note that a constant offset was applied to the salinities of profiles taken with the SBE-41CP CTD, that is, to the ARVOR and NINJA profiles, before computing  $\epsilon_{\text{new}}$ . The offset was based on a linear fit of the  $SP$  residual of the reference and float profiles in  $T$  space. Hydrographic variables (e.g.,  $CT$ ,  $CCo$ , etc.) are computed with the Gibbs Seawater package (McDougall & Barker, 2011).

The values of  $\epsilon_{\text{new}}$  and the constant offset are shown in Figure 2. Three of the four floats with a constant precalibration offset had an initial fresh bias, ranging from 0.0013 to 0.0187 psu, while one float had a saline

bias of 0.0013 psu.  $\epsilon_{\text{new}}$  values range from  $-14.909 \times 10^{-8}$  to  $-8.5686 \times 10^{-8}$  dbar $^{-1}$ . All values are within  $3.25 \times 10^{-8}$  dbar $^{-1}$  of the SBE-recommended value of  $-11.66 \times 10^{-8}$  dbar $^{-1}$  (i.e., differences are within 30% of the SBE-recommended value). After applying  $\epsilon_{\text{new}}$  and recalculating practical salinity, the float-mean *SP* residuals of the calibration profiles range from  $-0.0003$  psu to  $0.0001$  psu. All residuals over the stable part of the water column, calculated for the calibration profile for each float, remain less than  $\pm 0.006$  psu and cluster around 0 psu (Figure 2). 92% of the residuals are less than  $\pm 0.002$  psu. Thus, we conservatively estimate a practical salinity accuracy of  $\pm 0.005$  psu for Deep Argo floats in the AAB, and suggest a true accuracy likely closer to the Deep Argo program's targeted value of  $\pm 0.002$  psu. The accuracy of absolute salinity is then assumed to be  $\pm 0.005$  g kg $^{-1}$ , conservatively, and likely closer to  $\pm 0.002$  g kg $^{-1}$ .

#### 4. Methods

The Deep Argo floats provide remarkable spatial and temporal sampling coverage of bottom water in the AAB. We chose to define AABW as waters with  $\gamma^N > 28.30$  kg m $^{-3}$ , following van Wijk and Rintoul (2014). The distinction between RSBW and ALBW becomes apparent below this isopycnal, as the RSBW becomes more saline in the deeper, denser waters. There are 553 Deep Argo profiles that reach the top of the AABW layer, and AABW was detected near the seafloor in 408 of the 462 bottom-reaching profiles. These numbers exclude profiles taken by the Deep SOLO #7900679 and Deep NINJA #5905233 floats that exhibit a small, yet significant, drift. Note that some bottom-reaching profiles did not detect AABW.

Layer-mean AABW properties,  $SA_{\text{AABW}}$ ,  $CT_{\text{AABW}}$ ,  $\gamma_{\text{AABW}}^N$ , are calculated by averaging over the entire AABW layer of bottom-reaching profiles, that is, between the depth of the  $\gamma^N = 28.30$  kg m $^{-3}$  isopycnal and the seafloor. As vertical spacing of raw data can be irregular, mean properties are calculated after the data have been linearly interpolated to a 10-dbar pressure grid, such that data are evenly weighted with depth. The thickness of the AABW layer,  $H_{\text{AABW}}$ , is defined as the difference between the ocean bottom depth and the depth of the  $\gamma^N = 28.30$  kg m $^{-3}$  isopycnal. Note that  $H_{\text{AABW}}$  is calculated for all the profiles that sampled to any depth greater than the top of the AABW layer, not only those that reached the seafloor.

At first, we present an overview of AABW layer-mean properties in the AAB, followed by a more detailed look in regions near bottom water sources. The general distribution and variability of bottom water properties are mapped in the AAB by calculating the mean and standard deviation within a 2°-longitude by 1°-latitude grid, that is, in bins that span 2° of longitude and 1° of latitude. Along the slope, south of 61°S, we also investigate the along-isobath evolution of bottom water properties by averaging based on maximum pressure, that is, pressure at the seafloor, rather than latitude. This represents a more natural, flow-following coordinate system for the denser AABW layers ( $\gamma^N > 28.32$  kg m $^{-3}$ ). Note that only profiles that are known or assumed to have reached the seafloor are considered in this along-isobath analysis, as the data are sorted based on pressure at the seafloor, and we consider profiles with maximum pressures between 2,500 and 5,000 dbar. In regions near the sources of AABW, we provide a more detailed examination of bottom-reaching profiles. In particular, we look at regions near 140°E and 150°E, where direct comparison with shipboard hydrography collected over the past several decades helps interpret long-term trends and variability in the context of spatial variability of ALBW and RSBW.

ALBW and RSBW have distinct CT-SA curves (Rintoul, 1998; Thomas et al., 2020, see also the spread of abyssal CT-SA characteristics in Figure 1b). We use the shape of the CT-SA curve to determine where ALBW and RSBW are present or absent, and hence the pathways followed by the two varieties of AABW. RSBW is characterized by an abyssal salinity maximum, that is, increasing salinity with depth in its deepest layers (e.g., Jacobs & Giulivi, 2010). ALBW is characterized by cold bottom water and a near-linear CT-SA plot (e.g., Aoki et al., 2005; Gordon & Tchernia, 1978). Thus, where RSBW over-rides ALBW, a saline layer sits above a colder, fresher layer. Specifically, RSBW is present when bottom *SA* is 0.005 g kg $^{-1}$  greater than the *SA* on the 28.32 kg m $^{-3}$  isopycnal, and is considered particularly strong if the difference is greater than 0.01 g kg $^{-1}$ . A particularly weak signature of RSBW is identified when the difference is between 0.005 g kg $^{-1}$  and 0 g kg $^{-1}$  (i.e., deviating from the near-linear ALBW curves). The presence of ALBW is detected when *CT* <  $-0.5^\circ\text{C}$  at the bottom of the profile, and is considered particularly strong if *CT* <  $-0.55^\circ\text{C}$ . RSBW is present over ALBW when there is a local salinity maximum above the bottom (and the bottom temperature is less than  $-0.5^\circ\text{C}$ ). Note that we inspect the profiles on their original pressures in these regional analyses to avoid any impact of linear interpolation to an even pressure grid. Also note that this method allows for the inclusion of profiles taken by the two floats that exhibited a relatively



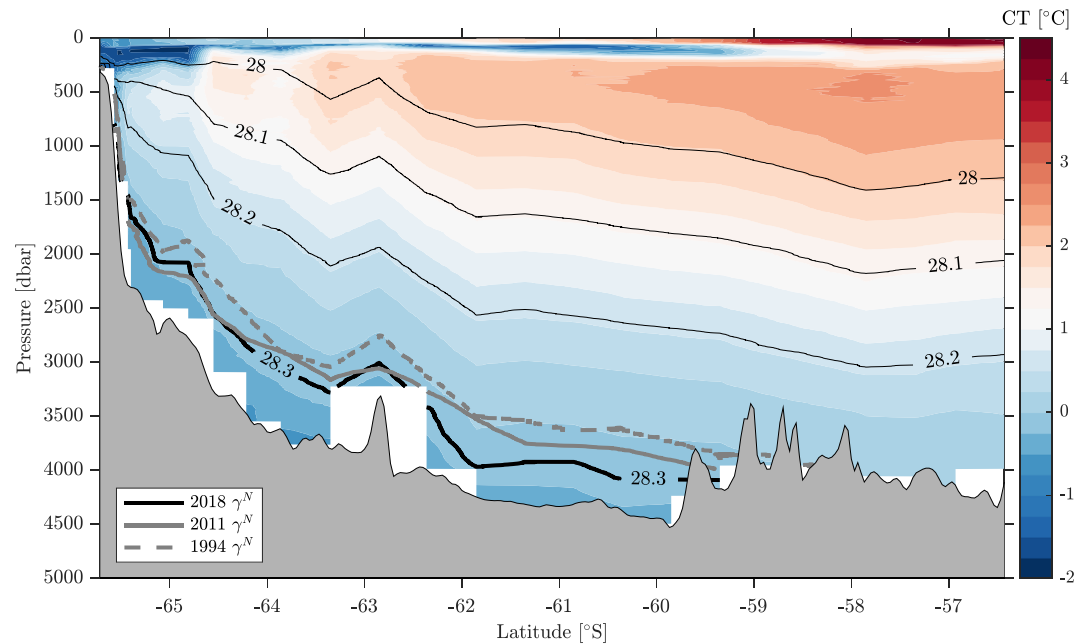


**Figure 3.** Temperature and density section along 140°E. Colors represent conservative temperature (CT) observed during the 2018 occupation of SR3, contoured every 0.25°C. Black lines show the isopycnal depths from 2018, with the thick line representing the top of the AABW layer ( $\gamma^N = 28.3 \text{ kg m}^{-3}$ ). Thick gray lines show the depth of the top of the AABW layer from two historical occupations of SR3: 2011 (solid line) and 1994 (dashed line). The contraction of the AABW layer over time can be seen by the deepening of the  $28.3 \text{ kg m}^{-3}$  isopycnal from 1994 through 2011 to 2018 across most of the section.

small drift toward fresher values, Deep SOLO #7900679 and Deep NINJA #5905233, as the shape of the CT-SA curves still provides valuable information.

## 5. Bottom Water Properties

Repeat shipboard hydrography provides invaluable information about the AABW layer, its shape, and how it has changed over the past few decades. The cold and dense waters, banked up against the continental slope, become thinner to the north. For example, in the AAB along 140°E, there is no AABW ( $\gamma^N > 28.3 \text{ kg m}^{-3}$ ) north of about 59°S (Figure 3). The AABW layer has contracted over time: the northern extent of the  $\gamma^N = 28.3 \text{ kg m}^{-3}$  isopycnal and the overall thickness of the layer have both decreased between 1994 and 2011 (Figure 3, gray lines). The 2018 occupation shows the AABW continued to contract offshore in waters deeper than about 3,000 m, roughly. However, inshore of the 3,000 m isobath, AABW layer thickness increased slightly between 2011 and 2018, after having decreased significantly between 1994 and 2011 (Figure 3).

Histograms of AABW layer-mean properties sampled by the Deep Argo floats are shown in Figure 4. There are some regional patterns in AABW properties, for example, the warmest AABW tend to be in the northern and southeastern part of the AAB (black and darker red bars in Figure 4a, respectively). However, while both varieties are thinner than AABW in the southwestern part of the basin (i.e.,  $H_{\text{AABW}}$  is generally less than 500 m, Figure 4d), the northern waters are lighter than those to the southeast (Figure 4c) and the southeastern waters are more saline than those to the north (Figure 4b). Finally, there is a large spread in  $SA_{\text{AABW}}$  and  $CT_{\text{AABW}}$  in the southern part of the basin (i.e., south of 61°S, colored bars in Figure 4). Warmer, saltier AABW indicative of RSBW is found to the east, whereas colder, fresher waters indicative of ALBW is found to the west. However, temperature and salinity variations in AABW tend to be density-compensated south of 61°S, where there is also general thickening of the AABW layer from east to west.

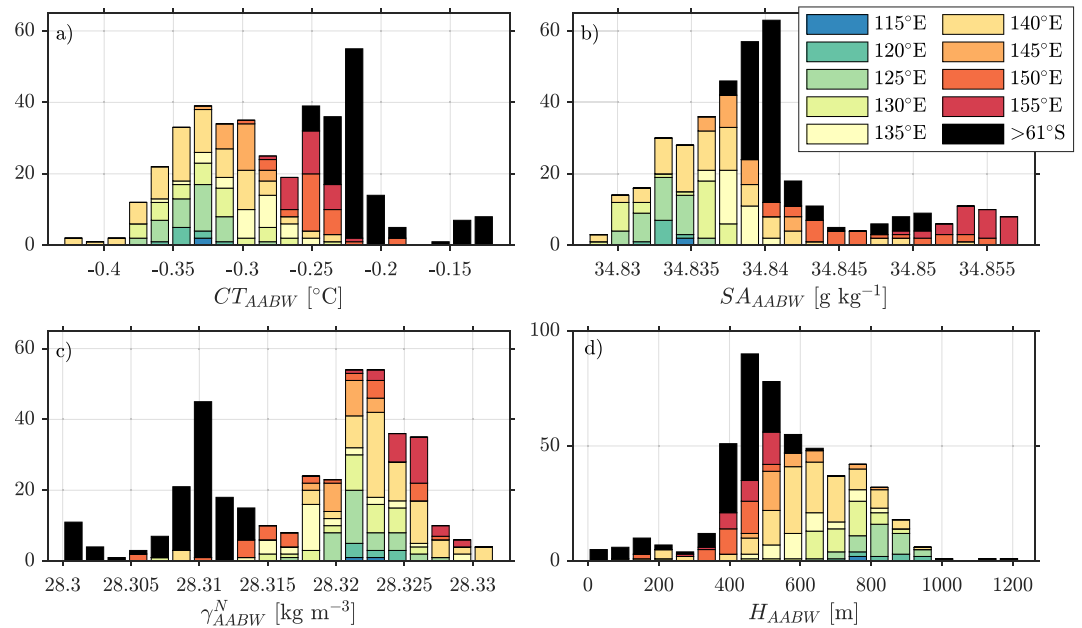


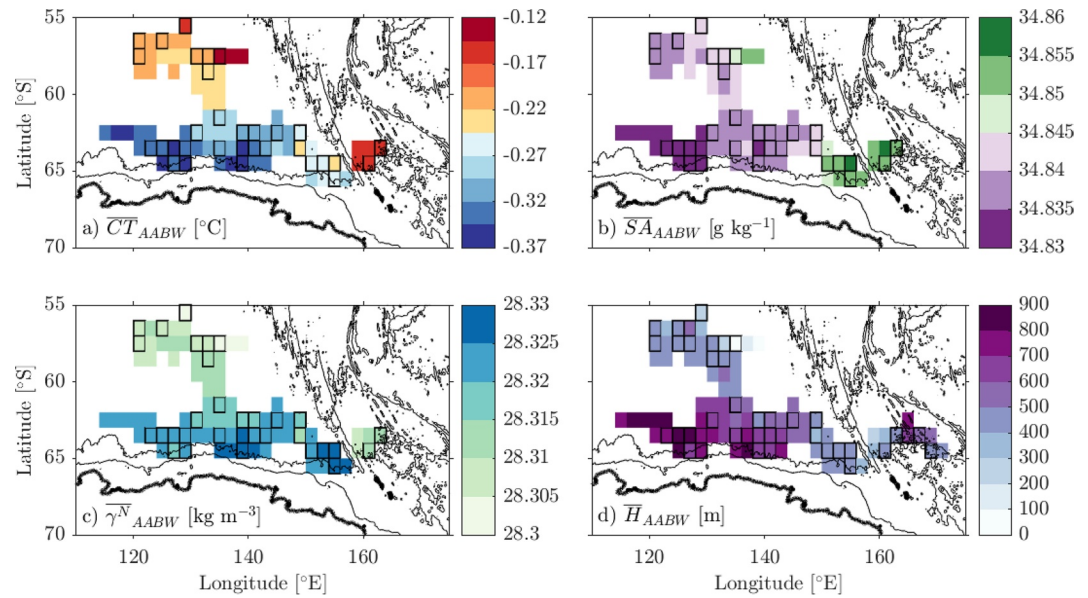
**Figure 4.** Histograms of layer-mean AABW properties in the AAB sampled by the Deep Argo floats. (a) Conservative temperature,  $CT_{AABW}$ ; (b) Absolute salinity,  $SA_{AABW}$ ; (c) Neutral density,  $\gamma_{AABW}^N$ ; (d) Layer thickness,  $H_{AABW}$ . Black bars represent profiles taken from the northern AAB, that is, all profiles north of  $61^\circ\text{S}$ . Colored bars represent profiles taken from the southern AAB, that is, profiles south of  $61^\circ\text{S}$  and west of  $158^\circ\text{E}$ , that are grouped into  $5^\circ$  bins of longitude. The longitude around which the bins are centered is given in the legend and colored such that dark red is to the east and dark blue to the west. Only bottom-reaching profiles are included in panels (a–c), while all profiles reaching the top of the AABW layer are included in panel (d). Note that profiles from outside the AAB, that is, all profiles east of  $158^\circ\text{E}$ , and data from the two floats that exhibited a small drift in salinity (Deep SOLO #7900679 and Deep NINJA #5905233) are not included in this figure. Also, note the different y-axis scale in panel (d).

### 5.1. Spatial Variability

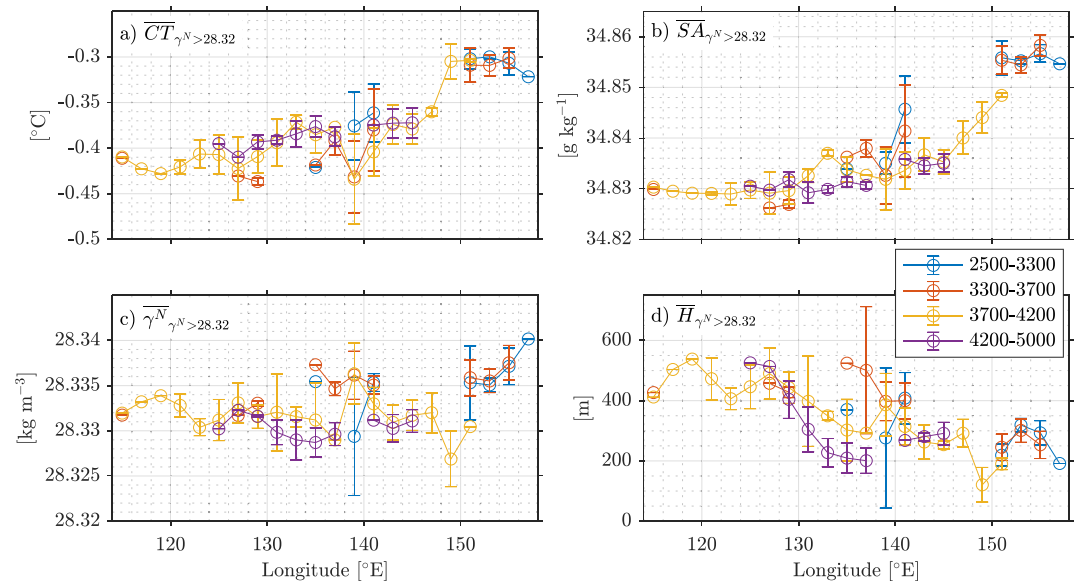
South of  $61^\circ\text{S}$ , the AABW layer cools, freshens, and thickens from east to west (Figure 5). East of about  $150^\circ\text{E}$ , the RSBW signature is clear, with elevated values of  $\overline{SA}_{AABW}$  and  $\overline{CT}_{AABW}$  (Figures 5a and 5b). Note that the overbar denotes the  $2^\circ$ -longitude by  $1^\circ$ -latitude averages of layer-mean AABW properties, for example,  $\overline{SA}_{AABW}$  is the mean of  $SA_{AABW}$  from all profiles with each bin. The coldest average AABW is found near  $140^\circ\text{E}$ , just downstream from the ALBW source (Figure 5a). In general, the standard deviation of  $CT_{AABW}$  and  $SA_{AABW}$  is less than  $0.025^\circ\text{C}$  and  $0.002\text{ g kg}^{-1}$ , respectively, for regions with five or more profiles (outlined in black, Figure 5). The exception is the elevated temperature and salinity variability near  $140^\circ\text{E}$ , where standard deviations are 2–3 times as high. This is where the ALBW and RSBW interact for the first time. That is, two water masses of similar densities, the cooler, fresher ALBW and warmer, saltier RSBW, are both present near  $140^\circ\text{E}$ , downstream of the Dense Shelf Water source flowing over the Adélie Sill. The AABW layer is thickest west of about  $130^\circ\text{E}$ , with  $\overline{H}_{AABW} > 700\text{ m}$  in general. The broad-brush patterns of AABW thickness are a general thickening to the west, as the basin gets deeper, and to the south, as the bottom waters are banked against the slope.

Figure 6 shows an along-isobath perspective of bottom water properties in the southern part of the AAB, that is, south of  $61^\circ\text{S}$ , and highlights the enhanced variability near  $140^\circ\text{E}$ . Note that here we show data west of  $158^\circ\text{E}$  and focus on the denser AABW layers, that is,  $\gamma^N > 28.32\text{ kg m}^{-3}$ , which are thought to reflect more recently produced AABW. In general, AABW progressively cools, freshens, and thickens westward along isobaths (Figure 6). However, there is enhanced variability in dense AABW properties downslope of the Adélie Land source of AABW near  $140^\circ\text{E}$ . It is here where we see a relatively large range of AABW properties across isobaths and relatively large standard deviations. For example, between  $138^\circ\text{E}$  and  $142^\circ\text{E}$ ,  $CT$  standard deviations range from  $0.026^\circ\text{C}$  to  $0.049^\circ\text{C}$  in the three shallowest depth bins, all of which contain between 3 and 31 profiles.

Between  $152^\circ\text{E}$  and  $158^\circ\text{E}$ , near the RSBW source and where the basin itself is shallower than  $3,700\text{ m}$ , AABW properties are independent of maximum pressure recorded by float (i.e., the red and blue circles overlap, Figure 6).



**Figure 5.** Mean AABW properties sampled by the Deep Argo floats ( $\gamma^N > 28.30 \text{ kg m}^{-3}$ ) averaged in  $1^\circ$  latitude  $\times$   $2^\circ$  longitude bins. (a) Conservative temperature,  $\overline{CT}_{AABW}$ ; (b) Absolute salinity,  $\overline{SA}_{AABW}$ ; (c) Neutral density,  $\overline{\gamma^N}_{AABW}$ ; (d) Layer thickness,  $\overline{H}_{AABW}$ . Only bottom-reaching profiles are included in panels (a–c), while all profiles reaching the top of the AABW layer are included in panel d, such that there is more data included in the latter. Data from the two floats that exhibited a small drift in salinity (Deep SOLO #7900679 and Deep NINJA #5905233) are not included in this figure. Regions with five or more profiles are outlined in black.



**Figure 6.** Mean dense water properties in the Australian-Antarctic Basin (AAB) sampled by the Deep Argo floats and grouped by maximum pressure, with the pressure ranges given in the legend. Here, dense water is defined as the layer denser than  $\gamma^N = 28.32 \text{ kg m}^{-3}$  (a) Conservative temperature,  $\overline{CT}_{\gamma^N > 28.32}$ ; (b) Absolute salinity,  $\overline{SA}_{\gamma^N > 28.32}$ ; (c) Neutral density,  $\overline{\gamma^N}_{\gamma^N > 28.32}$ ; (d) Layer thickness,  $\overline{H}_{\gamma^N > 28.32}$ . Error bars represent the standard deviation. Only profiles south of  $61^\circ\text{S}$  and west of  $158^\circ\text{E}$  are included. Only bottom-reaching profiles are included in all panels, as the data is sorted by maximum pressure at the seafloor. Data from the two floats that exhibited a small drift in salinity (Deep SOLO #7900679 and Deep NINJA #5905233) are not included in this figure.

Between 150°E and 152°E, profiles in deeper water (maximum pressures of 3,700–4,200 dbar) are about 0.01 g kg<sup>-1</sup> fresher and 0.005 kg m<sup>-3</sup> lighter than those in shallower water (yellow circles, Figures 6b and 6c). This suggests the main pathway of RSBW is along the slope and it does not descend all the way into the abyssal ocean upon entering the basin. Further, assuming a monotonic decrease in salinity westward from 150°E, the relatively high values of salinity in the shallower waters between 140°E and 142°E, suggest a continuation of the RSBW pathway to at least 140°E, with less RSBW in the deeper ocean.

One of the more striking patterns in the regional map of AABW properties is that, throughout the basin, there is relatively warm and buoyant AABW north of about 61°S (Figure 5). The AABW layers to the north are also relatively thin, with  $\bar{H}_{AABW}$  generally less than 500 m. It is around 61°–62°S where the isopycnals begin to strongly shoal, as the density layers begin to pile up against the continental slope to the south, as seen in Figure 3. AABW found north of the strong isopycnal shoaling has been largely modified by mixing with Circumpolar Deep Water from above, as they are found far from the sources of AABW and toward the end of their clockwise circuit around the AAB (McCartney & Donohue, 2007). Hence, AABW in the northern part of the basin is warmer, lighter, more saline, and thinner than that due south of it (Figure 5).

## 5.2. Temporal Variability

There has been a well-documented multi-decadal freshening trend in AABW throughout the AAB until the mid-2010s (Aoki et al., 2005, 2013; Menezes et al., 2017; Shimada et al., 2012; van Wijk & Rintoul, 2014). A recent salinity rebound has since been documented in Ross Sea DSW and RSBW (Castagno et al., 2019; Silvano et al., 2020; Thomas et al., 2020), as well more broadly in AABW throughout the AAB (Aoki et al., 2020). The Deep Argo floats also capture the westward spreading of the recently salinified RSBW, that is, an abyssal salinity maximum can be seen in *CT-SA* curves near 150°E (Figure 7 and Thomas et al., 2020). Ship-based profiles and Deep Argo float profiles from this region, shown in Figure 7b and found in the pink box in Figure 7a, were all taken to just above the seafloor during the austral summer (January–March). The RSBW sampled by Deep Argo floats in 2019 is more saline by about 0.01 g kg<sup>-1</sup> along the 28.32 kg m<sup>-3</sup> isopycnal than that in 2018. Note that although there is a continued increase in deep *SA* at 150°E, RSBW sampled in 2019 is thinner and less dense than that sampled in 2018 (Figure 7b). Additionally, 2019 profiles exhibit a weaker salinity tail than 2018 profiles, that is, a smaller difference between deep salinity minimum and bottom salinity. This suggests Deep Argo floats sampled more closely to the core of RSBW in 2018, while those more northern and deeper profiles in 2019 were farther from the main outflow pathway. Further, while the historical hydrography shows variability in the core of the RSBW outflow, that is, which of the three most repeated stations (orange squares in Figure 7a) has the highest abyssal salinity, it is typically found in either the southern or middle station (not shown).

In the southeast corner of the basin, east of 148° and south of 62°S, the floats also show a continuing increase in the RSBW salinity (Figure 7c). Note that the profiles shown here have all reached the seafloor and are taken throughout the year, with some having estimated under-ice positions, yet the results are similar if only profiles with known positions are used. On average, profiles taken to less than 3,700 dbar in 2019 and 2,020 are about 0.01 g kg<sup>-1</sup> higher in salinity on deep isopycnals than those in 2018, with those in 2020 slightly more saline than 2019. These profiles are almost all west of the western extent of the 3,700 m isobath (black, gray, and purple circles in Figure 7a) and a direct comparison to deeper profiles is not possible at these longitudes. However, profiles with maximum pressures greater than 3,700 dbar or north of 64°S are consistently fresher and less dense than profiles to less than 3,700 dbar from the same year (Figure 7c). Moreover, 2019 and 2020 profiles to greater than 3,700 dbar show fresher values of *SA* for  $\gamma^N > 27.32$  kg m<sup>-3</sup> than 2018 profiles with maximum pressures less than 3,700 dbar. This indicates the deep salinity rebound is strongest, and thus the main pathway of RSBW exists, along the mid-slope, inshore of 3,700 m isobath, consistent with the results above and Figure 7b.

The strongest signal of ALBW is found near 140°E, downstream of the DSW outflow over the Adélie Sill. This very cold and fresh (*CT* < -0.5°C, *SA* < 34.83) water is consistently found in the saddle south of the Hakurei Seamount and in depths greater than 3,500 m (Figure 8). We take the water in that saddle as representative of the core of ALBW. From the late 1990s through 2017, the ALBW core generally freshened (Figure 8b). There was also a cooling of the deepest waters through the 1990s, with the coldest and freshest abyssal waters observed in 2001 (purple lines). The densest layer of AABW was nonexistent in 2015 when  $\gamma^N < 28.34$  kg m<sup>-3</sup> everywhere in the region (brown lines). Shipboard profiles from the 2018 occupation of SR3 along 140°E revealed more slightly more saline waters than 2017 (seen by comparing the pink and gray lines), as do the Deep Argo float profiles

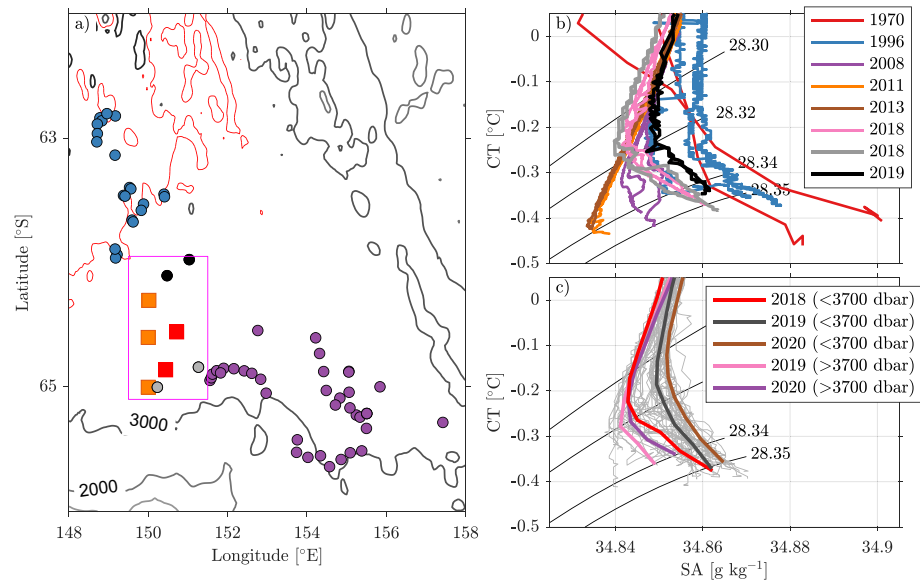


**Figure 7.** Variability of Ross Sea and Bottom Water (RSBW) near 150°E. (a) Map of the region near the repeat hydrographic transect. Grounded (known or assumed) Deep Argo profiles are shown as circles and select shipboard hydrography stations are shown as squares (red squares represent 1969 and 1971 profiles, orange represent profiles thereafter). Gray and black circles indicate Deep Argo profile locations from 2018 and 2019, respectively that are closest to the repeat hydrography locations (inside the pink box) and plotted in panel (b). Blue and purple circles indicate profiles from the broader region that are known or assumed to have reached the seafloor, reaching maximum pressures of greater or less than 3,700 dbar, respectively. Bathymetry is contoured every 1,000 meters with black lines and the 3,700 m isobath is in red. (b) Time evolution of profiles in  $CT$ - $SA$  space in the pink box. Gray and black lines represent Deep Argo profiles from 2018 and 2019, respectively, and correspond to circles in the pink box in panel (a). Colored lines represent shipboard hydrography, with the profile years given in the legend (profiles labeled 1970 are from 1969 and 1971). Note that all shipboard CTD profiles were taken between January and March, while Deep Argo profiles were taken in February and March. (c) Regional Deep Argo profiles in  $CT$ - $SA$  space shown as thin gray lines (all circles in panel a). Note that these are year-round profiles from 2018 to 2020 only. Mean profiles, averaged as a function of density, for each year are shown as thick lines. Thin black lines in panels b and c represent the  $\gamma^N = 28.30, 28.32, 28.34,$  and  $28.35 \text{ kg m}^{-3}$  isopycnals. Data from the two floats that exhibited a small drift in salinity (Deep SOLO #7900679 and Deep NINJA #5905233) are not included in this figure.

from summer 2019 (thick black lines). This is especially true along the  $\gamma^N = 28.34 \text{ kg m}^{-3}$  isopycnal, where the AABW is about  $0.02 \text{ g kg}^{-1}$  more saline in 2019 than it was in 2017.

There is much greater variability in AABW properties in the broader region around 140°E than in the bathymetry saddle (seen by comparing gray and green lines in Figure 8c). It is here, just downstream of the Adélie Sill, where ALBW and RSBW are interacting for the first time. The deep temperature and salinity, that is,  $CT$  and  $SA$  on the  $28.35 \text{ kg m}^{-3}$  isopycnals, range from about  $-0.4^\circ\text{C}$  to  $-0.7^\circ\text{C}$  and  $34.81 \text{ g kg}^{-1}$  to  $34.855 \text{ g kg}^{-1}$ , respectively. In addition to abyssal  $CT$  and  $SA$  values, the shape of the  $CT$ - $SA$  curves also exhibits enhanced variability. Some profiles show a local salinity maximum in the deep, either at the bottom of the profile or sitting atop colder, fresher ALBW; others have an approximately linear profile in  $CT$ - $SA$  space, indicative of pure ALBW. Note that the two profiles from the saddle region that appear to have some RSBW sitting atop ALBW are from winter and thus do not have known GPS positions, the positions of these profiles have been estimated using the under-ice navigation method of Wallace et al. (2020). However, it is plausible for the local variability to be such that it is not exclusively pure ALBW found there.

### 5.3. Case Study of Small-Scale Variability Near ALBW Source

Deep SOLO #7900636 provides an opportunity to investigate spatial and temporal variability of full-depth profiles over a small region just northwest of the Adélie Sill, where DSW flows off the shelf to supply ALBW (Figure 9). The float performed 17 near-daily profiles to the seafloor from 5 to 27 February 2019 over an area covering about 45 km in the zonal direction and 65 km in the meridional ( $140.69^\circ$ – $141.62^\circ\text{E}$  and  $63.6^\circ$ – $64.2^\circ\text{S}$ ; Figure 9a). All the profiles reached a similar depth range, recording maximum pressures between 3,815 dbar and

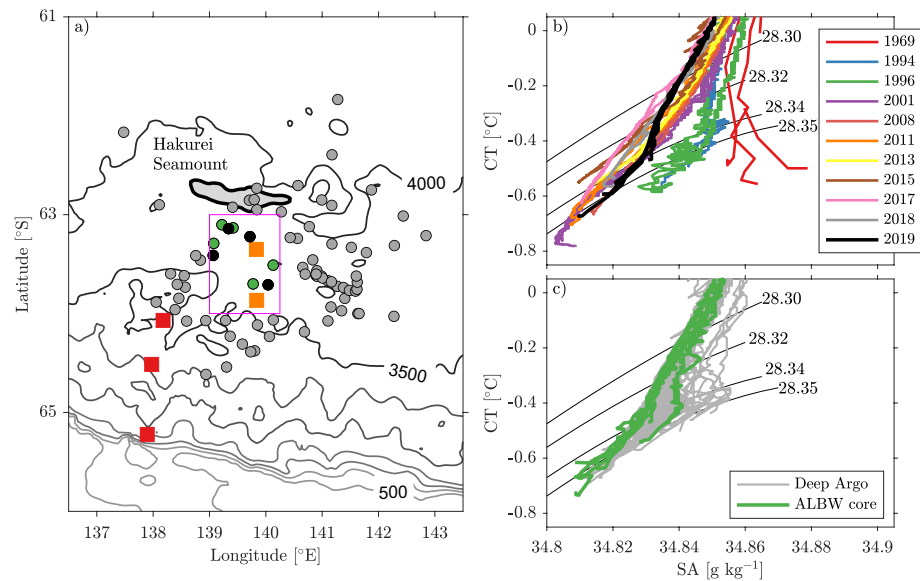


**Figure 8.** Variability near 140°E. (a) Map of the region near the SR3 repeat hydrographic transect along 140°. Grounded (known or assumed) Deep Argo profiles are shown as circles and select shipboard hydrography stations are shown as squares (red squares represent 1969 profiles, orange represent profiles thereafter). Black and green circles indicate grounded Deep Argo profiles taken in the saddle between the Hakurei Seamount to the north and continental slope, shown in green in panel (c). Note that the black circles represent summer profiles, that is, Deep Argo profiles from March to May 2019 and all have known position data, and the profiles represented by the green circles are from September to October 2018. Gray circles indicate profiles from the broader region that are known or assumed to have reached the seafloor. Bathymetry is contoured every 500 meters; the 3,500 m isobath around the Hakurei Seamount is in bold and the seamount is shaded in light gray. (b) Time evolution of profiles in  $CT-SA$  space. Black lines represent summer Deep Argo profiles and correspond to black circles in the pink box in panel (a). Note that all shipboard CTD data are from November through March, while summer Deep Argo profiles are from March to May. Colored lines represent shipboard hydrography, with the profile years given in the legend. (c) Regional Deep Argo profiles in  $CT-SA$  space shown as thin gray lines (all circles in panel a). Note that these are year-round profiles from 2018 to 2020 only. All profiles in the ALBW core south of the seamount (black and green circles in the pink box in panel a) are shown by the green lines, irrespective of month. Thin black lines in panels b and c represent the  $\sigma^N = 28.30, 28.32, 28.34, 28.35$  kg m<sup>-3</sup> isopycnals. Data from the two floats that exhibited a small drift in salinity (Deep SOLO #7900679 and Deep NINJA #5905233) are not included in this figure.

3,860 dbar, with the exception of the first two profiles that were shallower than 3,750 dbar. That is, after the first two southernmost profiles, the difference between maximum pressures is less than 45 dbar for all profiles shown. Note that the float trajectory does not necessarily represent deep flow, as the high frequency profiling causes the float to spend a relatively large fraction of its profiling cycle above the AABW layer and under the influence of the upper and midwater column flow. Also, note that after calibration, 89% of the salinity residuals between the calibration profile and the first deep profile taken by this float in the stable part of the water column are within  $\pm 0.002$  psu and only four residuals are greater than  $\pm 0.003$  psu. That is, the accuracy of profiles taken by this float is similar to the accuracy averaged over the entire array and reported in Section 3.2.

After taking an anticyclonic (counter-clockwise) path for its first eight profiles, from 140.7°E, 64.2°S to 140.9°E, 63.6°S, the float retraced its path back east-southeastward to 141.6°E, 63.8°S before turning almost due north to 141.6°E, 63.6°S (Figure 9a). Before its abrupt change in direction on 15 February, the float sampled AABW with minimum temperatures of  $-0.47^\circ\text{C} < CT < -0.51^\circ\text{C}$  (Figures 9b and 9c). Over the following four days, the float sampled AABW that was significantly colder and fresher at the bottom by up to  $0.1^\circ\text{C}$  and about  $0.01$  g kg<sup>-1</sup>, respectively (Figure 9d), in nearly the exact same locations as the previous few profiles. In fact, the initial appearance of this cold and fresh AABW between 15 and 16 February occurred between profiles taken only 15 km apart (Figure 9a). This suggests a pulse of ALBW appeared in that region in a matter of no more than 1 day and persisted for at least 3 days. The cold pulse had a thickness of about 60–90 m, that is, the  $-0.5^\circ\text{C}$  isotherm was 60–90 dbar above the seafloor on those 3 days. After 19 February, the float sampled AABW that had minimum temperatures similar to those taken before the pulse of ALBW (Figures 9d and 9e). However, this does not

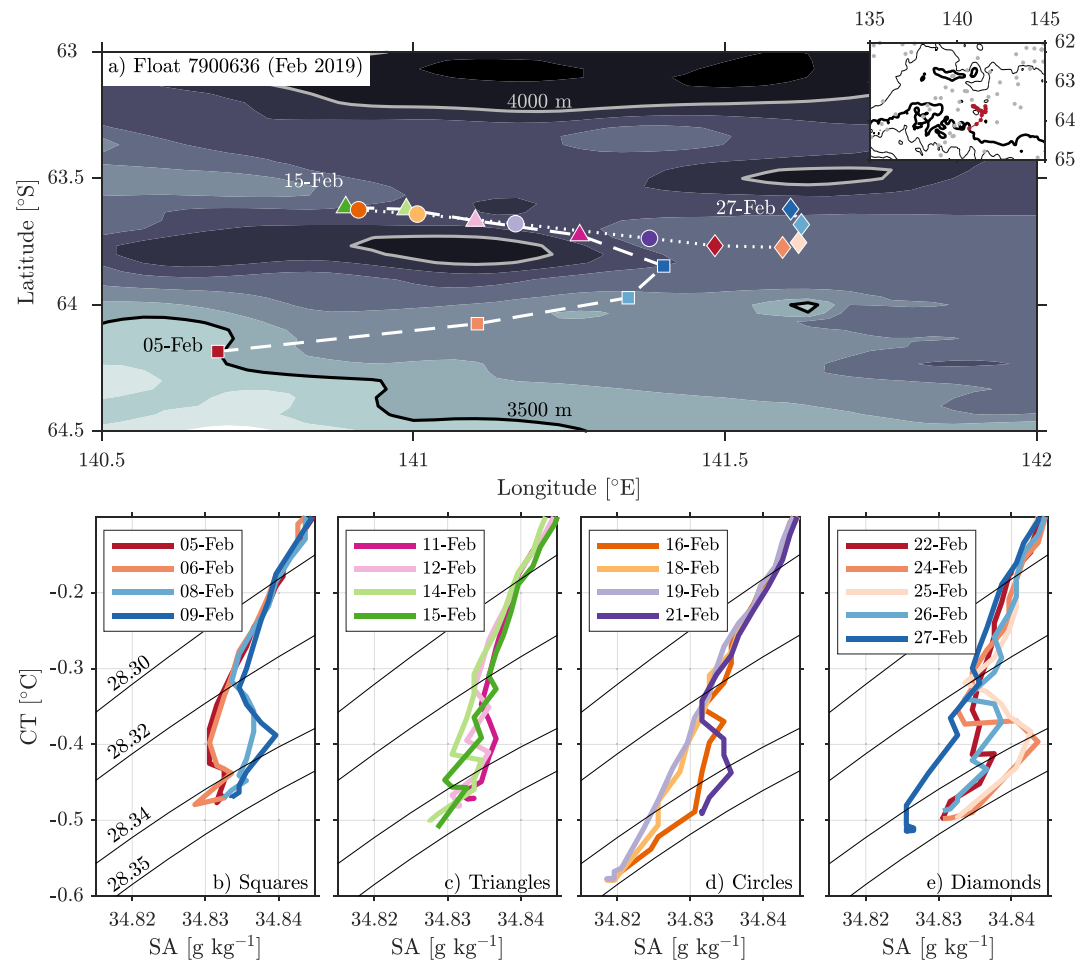


**Figure 9.** Case study of higher frequency variability and Ross Sea Bottom Water (RSBW)-Adélie Land Bottom Water (ALBW) interaction near Adélie Sill. (a) Map of near-daily profile locations, represented by colored symbols. The first half of the float's track shown with a dashed white line and the second half shown with a dotted white line. Bathymetry is shaded every 100 m, with the 3500-m isobath in black and the 4000-m isobath in gray. The inset on the top right corner shows the broader region and highlights the near-daily profiles in red. Bathymetry in the inset is contoured every 500 m; thick contour represents the 3500-m isobath. (b–e) Near-daily CT-SA diagrams in chronological order from panel b to panel (e). Profile color matches the marker color on the map in panel a, and associated marker shapes are written in bottom right corner of the CT-SA diagrams. Thin black lines in panels (b–e) represent the  $\gamma^N = 28.30, 28.32, 28.34, 28.35$  kg m<sup>-3</sup> isopycnals. Profile dates are given in the legends.

necessarily imply the pulse of ALBW was over after 3 days, as it is possible the float began profiling outside of the ALBW pathway and no longer observed the strong ALBW signal.

Profiles in Figures 9b–9e also show variability in the character of the warmer, saltier RSBW that sometimes, but not always, sits atop a layer of ALBW. The strongest signal of RSBW, with a deep SA maximum near 34.843 g kg<sup>-1</sup>, was found in two consecutive profiles near 141.6°E, 63.6°S on 24 and 25 February (Figure 9e). This roughly 200–300 m thick layer of RSBW is found at the bottom of the profile with a weak-to-no signal of ALBW below it, that is, SA > 34.83 g kg<sup>-1</sup> and CT > -0.55°C at the seafloor. A weaker and more variable RSBW layer of the same thickness, with deep SA maximum near 34.838 g kg<sup>-1</sup> and more wiggles in CT-SA space, is found in the profile immediately before and after those that sampled the strongest RSBW signal (22 and 26 February; Figure 9e). A day later, on 27 February, there is no sign of RSBW and a weaker ALBW is present (bottom CT < -0.5°C). Consistently, RSBW is found on the eastern side of this local trough rather than the western side or in the trough. There is only one instance where a thin layer of ALBW undercuts a thicker RSBW layer with a local salinity maximum of 34.835 g kg<sup>-1</sup>. That is, a 20 m thick layer of ALBW (SA < 34.83 g kg<sup>-1</sup> and CT < -0.5°C,

sampled by three data points) exists below a 200 m thick layer of RSBW on 16 February (Figure 9d). Note that this is the very beginning of the pulse of ALBW and that the subsequent profiles do not exhibit any RSBW.

## 6. Discussion

A Deep Argo pilot array provides the first seasonally unbiased view of AABW properties and pathways over a large swath of the Australian-Antarctic Basin. Consistent with previous analyses (e.g., Gordon & Tchernia, 1978; Orsi et al., 1999; Thomas et al., 2020; van Wijk & Rintoul, 2014), there is a distinct signature of two varieties of bottom water in the basin: RSBW and ALBW. The individual signatures of RSBW and ALBW are particularly strong close to their source regions in the Ross Sea and Adélie Land, respectively. The bottom salinity maximum that was characteristic of RSBW, and had disappeared in the 2000s after decades of freshening, has now returned to the AAB (Figure 7, Castagno et al., 2019; Silvano et al., 2020; Thomas et al., 2020). The linear  $CT-SA$  relationship characteristic of ALBW is also present, with slightly saltier values relative to the mid-2010s, especially near 140°E (Figure 8).

The map of AABW properties is consistent with the cyclonic circulation in the deep layers of the AAB, as inferred by McCartney and Donohue (2007). AABW cools and freshens from east to west in the southern part of the basin (Figures 5a and 5b), with a sharp jump in properties just downstream of the ALBW source. That is, the high salinity signature of RSBW is slowly eroded as it spreads westward from the Ross Sea source, and then diluted more strongly when it mixes with fresh ALBW. A mixture of the two AABW varieties is carried to the west along the continental slope and rise, around the basin, and ultimately returns eastward in the northern branch of the cyclonic circulation. Mixing of this AABW with overlying CDW produces warmer and more saline AABW observed north of 61°S. The thickest layers of AABW are found in the southwestern part of the sampled region (Figure 5d), where the deepest water is found and AABW pools up to form a thick layer.

The Deep Argo floats reveal the pathways and interaction between the two varieties of AABW with unprecedented spatial and temporal resolution. Figure 10 illustrates our interpretation of the pathways of ALBW and RSW along the slope. Profiles with nonlinear  $CT-SA$  curves and deep salinity maxima characteristic of RSBW are found as far west as 130°E, particularly in the deep boundary currents. West of 130°E, there are no profiles with a clear signature of RSBW. While the Deep Argo sampling is sparse, and we therefore cannot rule out the presence of RSBW farther west, historical hydrographic data has not revealed the signature of RSBW at 115°E, along I9S (e.g., Aoki et al., 2020; van Wijk & Rintoul, 2014). Thus, we infer that distinct characteristics of RSBW and ALBW have been mixed away by 115°E, and possibly even by 130°E.

The main pathway of RSBW appears to follow the middle part of the continental slope ( $P_{\max} < 3,700$  dbar), with a strong signal of RSBW found as far west as 140°E (Figure 10a, large red triangles). That is, profiles showing an increase in  $SA$  greater than  $0.01 \text{ g kg}^{-1}$  between the  $\gamma^N = 28.32 \text{ kg m}^{-3}$  isopycnal and the bottom are found between 160°E and 140°E. Signs of strong RSBW are found deeper in the basin near 150°E, however the continued rebound of RSBW salinity (Castagno et al., 2019; Silvano et al., 2020) is stronger in profiles inshore of the 3,700 m isobath than it is in deeper profiles in the southeast corner of the basin (Figure 7c). These patterns imply RSBW flowing out of the main pathway and into the deeper ocean, as indicated by the small red arrows in Figure 10b. The mechanism for this leakage is unknown. We suspect that eddies, the influence of tides, and/or canyons on the seafloor that channel some RSBW to the deep ocean likely play a role in transporting RSBW out of its main pathway. There could be a few localized pathways of RSBW down the slope, like those observed near 150°E and 140°–145°E, or it could be happening everywhere along the slope. The gap in data near 64°S and 145°–150°E due to the random sampling by Deep Argo floats (Figure 10a) prohibits us from saying confidently whether or not RSBW is leaking into the deep ocean there. The semi-transparent red arrow in Figure 10b represents that possibility. The waters that entered the deep ocean eventually make their way around the northern side of the seamount, where we find a very weak signal of RSBW (Figure 10a, small pink triangles).

There is a remarkable amount of variability in the AABW properties near 140°E, where ALBW and RSBW first intersect (Figures 8c and 10a). In this area, there are profiles that observe only ALBW (nearly linear in  $CT-SA$  space, blue squares), only RSBW (increasing salinity at bottom of profile, red triangles), and the presence of both (ALBW underneath RSBW, seen as a local salinity maximum above the bottom, red dots on blue squares). However, the properties of AABW found between the continental slope and the Hakurei Seamount near 63°S consistently reflect ALBW only. That is, the core of ALBW flows down from the Adélie Sill, near 145°E, and



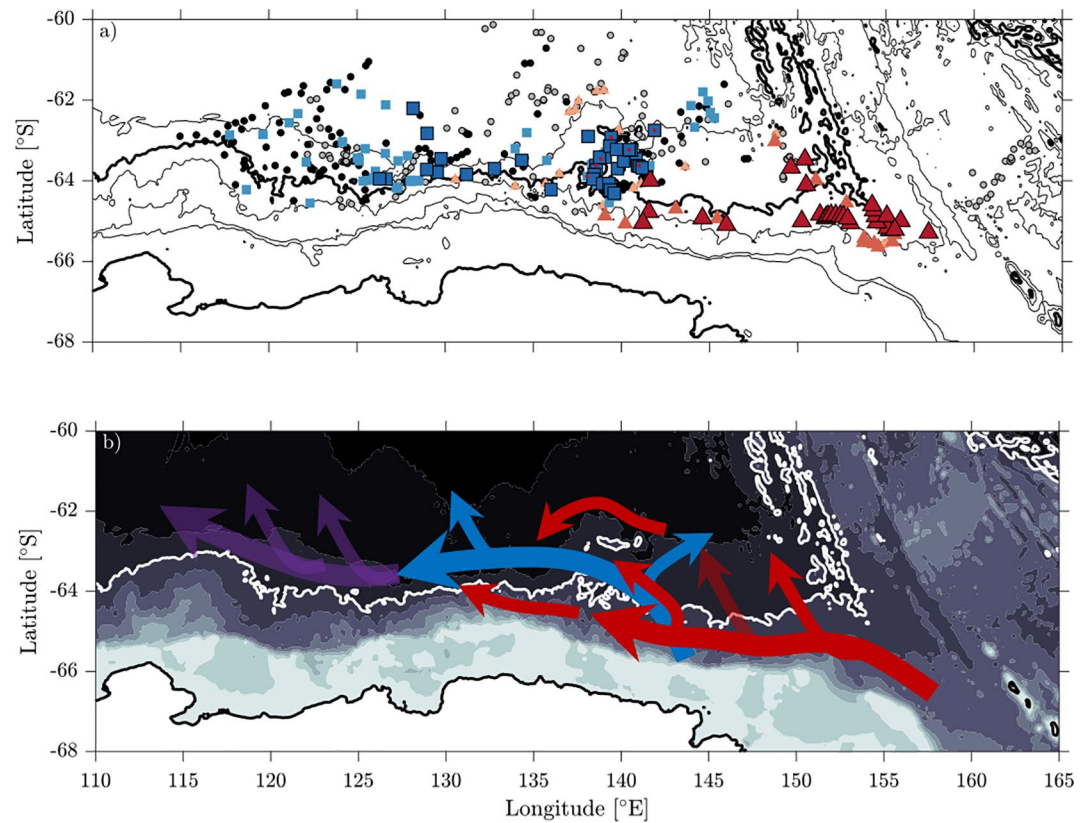


**Figure 10.** Ross Sea Bottom Water (RSBW) and Adélie Land Bottom Water (ALBW) pathways. (a) Locations of all profiles that reached the seafloor (known or assumed to be grounded) are shown by the gray dots; profiles with dense AABW present (maximum  $\gamma^N > 28.34 \text{ kg m}^{-3}$ ) are shown as black dots. Colored markers indicate the two flavors of AABW: RSBW (red triangles) and ALBW (blue squares). RSBW, with bottom  $SA$  greater than  $SA$  on the  $28.32 \text{ kg m}^{-3}$  isopycnal by at least  $0.005 \text{ g kg}^{-1}$ , is shown as red triangles. Larger triangles indicate profiles with particularly strong RSBW (deep salinity increases by more than  $0.01 \text{ g kg}^{-1}$ ) and smaller triangles indicate weak RSBW (deep salinity increases by less than  $0.005 \text{ g kg}^{-1}$ ). ALBW, with bottom  $CT < -0.5^\circ\text{C}$  shown as blue squares; larger squares indicate particularly strong ALBW (bottom  $CT < -0.55^\circ\text{C}$ ). Red dots indicate profiles that sampled RSBW above ALBW (defined as a local salinity max above the bottom and  $CT < -0.5^\circ\text{C}$  at the bottom). Bathymetry is contoured every 1,000 meters, with the Antarctic coast in bold. The 3500-m isobath is also plotted in bold. (b) Schematic representation of AABW pathways. Red and blue arrows illustrate pathways of RSBW and ALBW, respectively, from the two source regions. The purple arrows indicate where neither of the two varieties of AABW have a particularly strong signal. The main pathways are represented by the larger arrows and thinner arrows represent deviations from this main pathway; semi-transparent arrows represent possible pathways. Bathymetry is contoured on a greyscale every 500 m, with the bold lines representing the Antarctic coast (black) and the 3500-m isobath (white).

south of the seamount (Figure 10b, large blue arrow). Profiles north of the seamount do not display any bottom water colder than  $-0.55^\circ\text{C}$ , except one that is nearly due east, implying the vast majority of the ALBW navigates through the saddle south of the seamount. There is some slightly warmer ALBW (bottom  $CT < -0.5^\circ\text{C}$ ) found to the northeast near  $145^\circ\text{E}$  and  $62^\circ\text{S}$  (Figure 10a). Again, we assume that this is due to some leakage out of the main pathway due to eddies, tidal interactions, and/or channeling of dense water down deep-sea canyons.

The bathymetric saddle between the Hakurei Seamount and the continental slope, where we find the core of ALBW not far from its DSW source, is ideal for tracking long-term changes in ALBW properties. Conveniently, this is along the SR3 repeat hydrography transect, one of the most frequently occupied WOCE/GO-SHIP sections. Observations show ALBW has freshened since the early 1990s (van Wijk & Rintoul, 2014) and began salinifying in the mid 2010s (Aoki et al., 2020). The Deep Argo float data shows that ALBW salinity has continued to increase through 2019, consistent with Aoki et al. (2020), especially in waters denser than  $28.32 \text{ kg m}^{-3}$  (Figure 8b). Further, that the deep floats show this saddle region contains the purest ALBW relative to the broader region (Figure 8c) provides confidence that the long-term trends observed in shipboard hydrography there are

tracking changes in ALBW properties. However, it is perhaps not appropriate to include the 1969 profiles in very local trends of ALBW properties. Taken together, the along-slope pathway of RSBW seen by the deep floats (Figure 10) and the deep salinity maxima seen in those profiles (red lines, Figure 8b) suggest that the *Eltanin* profiles may have sampled the extension of the RSBW pathway rather than ALBW. Of course, the other profiles taken from the 1969–1971 in other regions of the AAB are appropriate to include when considering long-term trends of AABW more broadly in the basin (e.g., van Wijk & Rintoul, 2014). It is only those very local trends near 140°E that may be comparing a different water mass in 1969 to that sampled for the rest of the time series, that is, RSBW in 1969 and ALBW thereafter.

The interaction between ALBW and RSBW, and high-frequency variability where these two water masses intersect, is highlighted in an opportunistic case study of near-daily profiles taken over a small region near 141°E, 64°S (Figure 9). Pulsing of ALBW from its source region is illustrated by the sudden appearance of bottom water on 16 February 2019 that is more than 0.5°C colder and almost 0.01 fresher than a nearly co-located profile from the previous day. This ALBW layer, with bottom  $CT \approx -0.58^\circ\text{C}$  and  $SA \approx 34.82 \text{ g kg}^{-1}$ , is present for at least three days. We cannot say for certain whether the pulse ended after three days or the float drifted away from the plume. Yet, we can say with confidence that the nearly colocated profiles taken 11–15 February did not observe bottom water as cold or fresh as that. Mooring data also shows high-frequency variability in current speed and near-bottom temperature in this region (Fukamachi et al., 2000), further suggesting the outflow of ALBW occurs in pulses rather than a consistent flow. Fukamachi et al. (2000) estimate a 20-day transit time from the center of the Mertz polynya to their mooring at about 65°S, 140°E, thus this pulse of ALBW was likely formed in January 2019, indicating summertime DSW formation and export. High-resolution modeling work will be useful to tease out the driver(s) of these down-slope pulses of ALBW, be it tides, eddies, and/or local wind variability.

## 7. Conclusion

A pilot array of 12 Deep Argo floats provides seasonally unbiased information about the properties of AABW by simultaneously sampling a large swath of the Australian-Antarctic Basin. These floats are able to profile to the seafloor (as deep as 6,000 or 4,000 dbar, depending on the float model) and underneath the winter sea ice layer. A general cyclonic (clockwise) circulation of AABW, westward from its sources in the Ross Sea and Adélie Land, is inferred from the float data, and is consistent with previous studies. However, the float data illuminate the pathways of RSBW and ALBW in greater detail than previously possible from historical data. The main pathway of RSBW flows inshore of the 3,700 m isobath, and is present to about 130°E (Figure 10); the strongest, that is, purest, ALBW signal is found in the bathymetric saddle between the continental slope and seamount at 63°S at 140°E. The mechanisms for leakage from these main pathways into the deep basin is unknown, yet we hypothesize that deep eddies are the main driver. The incidental near-daily profiling of one Deep Argo float shows highly enhanced variability near 141°E and 64°S indicative of pulsing of ALBW from the shelf during Austral summer. In addition to describing the general properties, and spatial and temporal variability, of AABW in the Australian-Antarctic Basin, this study also highlights some of the possibilities that are sure to arise with the maintenance and growth of the Deep Argo program.

## Data Availability Statement

All data are publicly available. Deep Argo data were collected and made freely available by the international Argo Program and the national programs that contribute to it (<http://www.argo.ucsd.edu>, <http://argo.jcommops.org>, <https://nrlgodae1.nrlmry.navy.mil/argo/argo.html>). The ship-based hydrography used in this study are publicly available from the Clivar and Carbon Hydrographic Data Office (CCHDO; <http://cchdo.ucsd.edu>), with the exception of 140°E occupations in 2013, 2015, and 2017, which are available from the Australian Antarctic Data Centre (<https://data.aad.gov.au/aadc/>) under voyage names ta1302, au1402, and au1602, respectively. A large portion of the ship-based hydrography was collected and made publicly available by the International Global Ship-based Hydrographic Investigations Program (GO-SHIP; <http://www.go-ship.org>). ETOPO2v2 bathymetry data are also freely available through NOAA's National Centers for Environmental Information (<https://www.ngdc.noaa.gov/mgg/global/etopo2.html>).

### Acknowledgments

The authors thank the captains, crews, and scientists of the research vessels for their part in collecting the shipboard hydrography and deploying the Deep Argo floats. They also thank R. Cowley and R. Scott for their help in processing and piloting the MRV Deep SOLO floats; the SIO's Argo team for their efforts; and S. Le Reste, V. Thierry, G. Maze, and N. Poffa for their continuing support regarding Deep Arvor floats. A. Foppert and S. R. Rintoul were supported by the Centre for Southern Hemisphere Oceans Research, a partnership between the Commonwealth Scientific and Industrial Research Organisation and the Qingdao National Laboratory for Marine Science. A. Foppert, S. R. Rintoul, and E. M. van Wijk were supported by the Australian Antarctic Program Partnership (AAPP) through grant funding from the Australian Government as part of the Antarctic Science Collaboration Initiative program. S. R. Rintoul and E. M. van Wijk were also supported by the Australian Government's National Environmental Science Program. SGP, NZ, and the SIO Deep Argo floats were supported by NOAA Grant NA15OAR4320071. T. Kobayashi was supported by Grant-In-Aid for Scientific Research (19K03981) of the MEXT of the Japanese Government. J. B. Sallée received funding from the European Union's Horizon 2020 Research and Innovation programme under grant agreement number 821001. Deep Arvor floats were developed and funded through the EQUIPEX NAOS project funded by the French National Research Agency (ANR) under reference ANR-10-EQPX-40.

### References

- Aoki, S., Kitade, Y., Shimada, K., Ohshima, K. I., Tamura, T., Bajish, C. C., et al. (2013). Widespread freshening in the seasonal ice zone near 14°E off the Adélie Land coast, Antarctica, from 1994 to 2012. *Journal of Geophysical Research*, *118*(11), 6046–6063. <https://doi.org/10.1002/2013JC009009>
- Aoki, S., Rintoul, S. R., Ushio, S., Watanabe, S., & Bindoff, N. L. (2005). Freshening of the Adélie Land bottom water near 14°E. *Geophysical Research Letters*, *32*(23), 1–4. <https://doi.org/10.1029/2005GL024246>
- Aoki, S., Yamazaki, K., Hirano, D., Katsumata, K., Shimada, K., Kitade, Y., et al. (2020). Reversal of freshening trend of Antarctic bottom water in the Australian-Antarctic Basin during 2010s. *Scientific Reports*, *10*(1), 1–7. <https://doi.org/10.1038/s41598-020-71290-6>
- Boyer, T. P., Baranova, O. K., Coleman, C., Garcia, H. E., Grodsky, A., Locarnini, R. A., et al. (2018). *World Ocean database 2018*. NOAA Atlas NESDIS.
- Castagno, P., Capozzi, V., DiTullio, G. R., Falco, P., Fusco, G., Rintoul, S. R., et al. (2019). Rebound of shelf water salinity in the Ross Sea. *Nature Communications*, *10*(1), 1–6. <https://doi.org/10.1038/s41467-019-13083-8>
- Fukamachi, Y., Wakatsuchi, M., Taira, K., Kitagawa, S., Ushio, S., Takahashi, A., et al. (2000). Seasonal variability of bottom water properties off Adélie Land, Antarctica. *Journal of Geophysical Research: Oceans*, *105*(C3), 6531–6540. <https://doi.org/10.1029/1999jc900292>
- Gordon, A. L., & Tchernia, P. (1978). Waters of the continental margin off Adélie coast, Antarctica. In D. E. Hayes (Ed.), *Antarctic research series* (pp. 59–69). <https://doi.org/10.1029/AR019p0059>
- Jackett, D. R., & McDougall, T. J. (1997). A neutral density variable for the world's oceans. *Journal of Physical Oceanography*, *27*(2), 237–263. [https://doi.org/10.1175/1520-0485\(1997\)027<0237:andvft>2.0.co;2](https://doi.org/10.1175/1520-0485(1997)027<0237:andvft>2.0.co;2)
- Jacobs, S. S., & Giulivi, C. F. (2010). Large multidecadal salinity trends near the Pacific-Antarctic continental margin. *Journal of Climate*, *23*(17), 4508–4524. <https://doi.org/10.1175/2010JCLI3284.1>
- Joyce, T. M. (1994). *Introduction to the collection of expert reports compiled for the WHP programme (Tech. Rep. Nos. WHP operations and methods, WOCE operations manual, WHP Office report)*. Woods Hole Oceanographic Institution.
- Kobayashi, T. (2018). Rapid volume reduction in Antarctic Bottom water off the Adélie/George V Land coast observed by deep floats. *Deep-Sea Research Part I: Oceanographic Research Papers*, *140*, 95–117. <https://doi.org/10.1016/j.dsr.2018.07.014>
- Kobayashi, T., Sato, K., & King, B. A. (2021). Observed features of salinity bias with negative pressure dependency for measurements by SBE 41CP and SBE 61 CTD sensors on deep profiling floats. *Progress in Oceanography*, *198*, 102686. <https://doi.org/10.1016/j.pocean.2021.102686>
- Kobayashi, T., Watanabe, K., & Tachikawa, M. (2013). Deep NINJA collects profiles down to 4,000 meters. *Sea Technology*, *54*, 41–44.
- Le Reste, S., Dutreuil, V., André, X., Thierry, V., Renaut, C., Le Traon, P. Y., & Maze, G. (2016). “Deep-Arvor”: A new profiling float to extend the Argo observations down to 4000-m depth. *Journal of Atmospheric and Oceanic Technology*, *33*(5), 1039–1055. <https://doi.org/10.1175/JTECH-D-15-0214.1>
- McCartney, M. S., & Donohue, K. A. (2007). A deep cyclonic gyre in the Australian-Antarctic Basin. *Progress in Oceanography*, *75*(4), 675–750. <https://doi.org/10.1016/j.pocean.2007.02.008>
- McDougall, T. J., & Barker, P. M. (2011). *Getting started with TEOS-10 and the Gibbs Seawater (GSW) oceanographic Toolbox*. SCOR/IAPSO WG127.
- Menezes, V. V., Macdonald, A. M., & Schatzman, C. (2017). Accelerated freshening of Antarctic Bottom Water over the last decade in the southern Indian Ocean. *Science Advances*, *3*(1), 1–10. <https://doi.org/10.1126/sciadv.1601426>
- National Geophysical Data Center. (2006). *2-minute gridded global relief data (ETOPO2) v2*. National Geophysical Data Center, NOAA. <https://doi.org/10.7289/V5J1012Q>
- Orsi, A. H., Johnson, G. C., & Bullister, J. L. (1999). Circulation, mixing, and production of Antarctic bottom water. *Progress in Oceanography*, *43*(1), 55–109. [https://doi.org/10.1016/S0079-6611\(99\)00004-X](https://doi.org/10.1016/S0079-6611(99)00004-X)
- Purkey, S. G., & Johnson, G. C. (2010). Warming of global abyssal and deep Southern Ocean waters between the 1990s and 2000s: Contributions to global heat and sea level rise budgets. *Journal of Climate*, *23*(23), 6336–6351. <https://doi.org/10.1175/2010JCLI3682.1>
- Purkey, S. G., & Johnson, G. C. (2012). Global contraction of Antarctic bottom water between the 1980s and 2000s. *Journal of Climate*, *25*(17), 5830–5844. <https://doi.org/10.1175/JCLI-D-11-00612.1>
- Purkey, S. G., & Johnson, G. C. (2013). Antarctic bottom water warming and freshening: Contributions to sea level rise, ocean freshwater budgets, and global heat gain. *Journal of Climate*, *26*(16), 6105–6122. <https://doi.org/10.1175/JCLI-D-12-00834.1>
- Rintoul, S. R. (1998). On the origin and influence of Adélie Land bottom water. In S. S. Jacobs & R. F. Weiss (Eds.), *Ocean, ice, and atmosphere: Interactions at the Antarctic continental margin* (pp. 151–171). American Geophysical Union. <https://doi.org/10.1029/ar075p0151>
- Roemmich, D., Sherman, J. T., Davis, R. E., Grindley, K., McClune, M., Parker, C. J., et al. (2019). Deep SOL: A full-depth profiling float for the Argo program. *Journal of Atmospheric and Oceanic Technology*, *36*(10), 1967–1981. <https://doi.org/10.1175/JTECH-D-19-0066.1>
- Shadwick, E. H., Rintoul, S. R., Tilbrook, B., Williams, G. D., Young, N., Fraser, A. D., et al. (2013). Glacier tongue calving reduced dense water formation and enhanced carbon uptake. *Geophysical Research Letters*, *40*(5), 904–909. <https://doi.org/10.1002/grl.50178>
- Shimada, K., Aoki, S., Ohshima, K. I., & Rintoul, S. R. (2012). Influence of Ross Sea bottom water changes on the warming and freshening of the Antarctic bottom water in the Australian-Antarctic Basin. *Ocean Science*, *8*(4), 419–432. <https://doi.org/10.5194/os-8-419-2012>
- Silvano, A., Foppert, A., Rintoul, S. R., Holland, P. R., Tamura, T., Kimura, N., & Macdonald, A. M. (2020). Recent recovery of Antarctic bottom water formation in the Ross Sea driven by climate anomalies. *Nature Geoscience*, *13*, 1–7. <https://doi.org/10.1038/s41561-020-00655-3>
- Snow, K., Rintoul, S. R., Sloyan, B. M., & Hogg, A. M. C. (2018). Change in dense shelf water and Adélie land bottom water precipitated by iceberg calving. *Geophysical Research Letters*, *45*(5), 2380–2387. <https://doi.org/10.1002/2017GL076195>
- Thomas, G., Purkey, S. G., Roemmich, D., Foppert, A., & Rintoul, S. R. (2020). Spatial variability of Antarctic bottom water in the Australian Antarctic Basin from 2018–2020 captured by Deep Argo. *Geophysical Research Letters*, *47*. <https://doi.org/10.1029/2020gl089467>
- van Wijk, E. M., & Rintoul, S. R. (2014). Freshening drives contraction of Antarctic bottom water in the Australian Antarctic Basin. *Geophysical Research Letters*, *41*(5), 1657–1664. <https://doi.org/10.1002/2013GL058921>
- Wallace, L. O., van Wijk, E. M., Rintoul, S. R., & Hally, B. (2020). Bathymetry-constrained navigation of Argo floats under sea ice on the Antarctic continental shelf. *Geophysical Research Letters*, *47*(11), 1–9. <https://doi.org/10.1029/2020GL087019>
- Yamazaki, K., Aoki, S., Shimada, K., Kobayashi, T., & Kitade, Y. (2020). Structure of the subpolar Gyre in the Australian-Antarctic Basin derived from Argo floats. *Journal of Geophysical Research: Oceans*, *125*(8). <https://doi.org/10.1029/2019JC015406>
- Zilberman, N., King, B. A., Purkey, S., Thierry, V., & Roemmich, D. (2019). *Report on the 2nd deep Argo implementation workshop (Tech. Rep. No. May)*. Hobart, Australia. Retrieved from <https://argo.ucsd.edu/wp-content/uploads/sites/361/2020/04/DAIW2report.pdf>